Cell Reports, Volume *36*

Supplemental information

Agonists and allosteric modulators promote signaling from different metabotropic glutamate receptor 5 conformations

Chady Nasrallah, Giuseppe Cannone, Julie Briot, Karine Rottier, Alice E. Berizzi, Chia-Ying Huang, Robert B. Quast, Francois Hoh, Jean-Louis Banères, Fanny Malhaire, Ludovic Berto, Anaëlle Dumazer, Joan Font-Ingles, Xavier Gómez-Santacana, Juanlo Catena, Julie Kniazeff, Cyril Goudet, Amadeu Llebaria, Jean-Philippe Pin, Kutti R. Vinothkumar, and Guillaume Lebon

Supplementary information

Agonists and allosteric modulators promote signalling from different metabotropic glutamate receptor 5 conformations [115]

Chady Nasrallah[1,9], Giuseppe Cannone[2,9], Julie Briot[1,9], Karine Rottier[1], Alice E. Berizzi[1], Chia-Ying Huang [3], Robert B. Quast[4], Francois Hoh[4], Jean-Louis Banères[5], Fanny Malhaire[1] Ludovic Berto[1], Anaëlle Dumazer[1], Joan Font-Ingles[6], Xavier Gómez-Santacana[1,6], Juanlo Catena[6,7], Julie Kniazeff[1], Cyril Goudet[1], Amadeu Llebaria[6], Jean-Philippe Pin[1], Kutti R. Vinothkumar[8]*, Guillaume Lebon[1,10]*.

[1] IGF, Université de Montpellier, CNRS, INSERM, 34094, Montpellier, France

[2] MRC Laboratory of Molecular Biology, Cambridge, CB2 0QH, UK

[3] Swiss Light Source, Paul Scherrer Institute, CH-5232, Villigen, Switzerland

[4] CBS, Université de Montpellier, CNRS, INSERM, 34094, Montpellier, France

[5] IBMM, Université de Montpellier, CNRS, ENSCM, 34093, Montpellier, France

[6] MCS, Laboratory of Medicinal Chemistry and Synthesis, Institute of Advanced Chemistry of Catalonia (IQAC-CSIC), Barcelona, Spain.

[7] SIMChem, Synthesis of High Added Value Molecules, Institute of Advanced Chemistry of Catalonia (IQAC-CSIC), Barcelona, Spain

[8] National Centre for Biological Sciences TIFR, GKVK Post, Bellary Road, Bangalore, 560065, India

[9] These authors contributed equally

[10] Lead Contact

*Correspondence to: vkumar@ncbs.res.in ; guillaume.lebon@igf.cnrs.fr

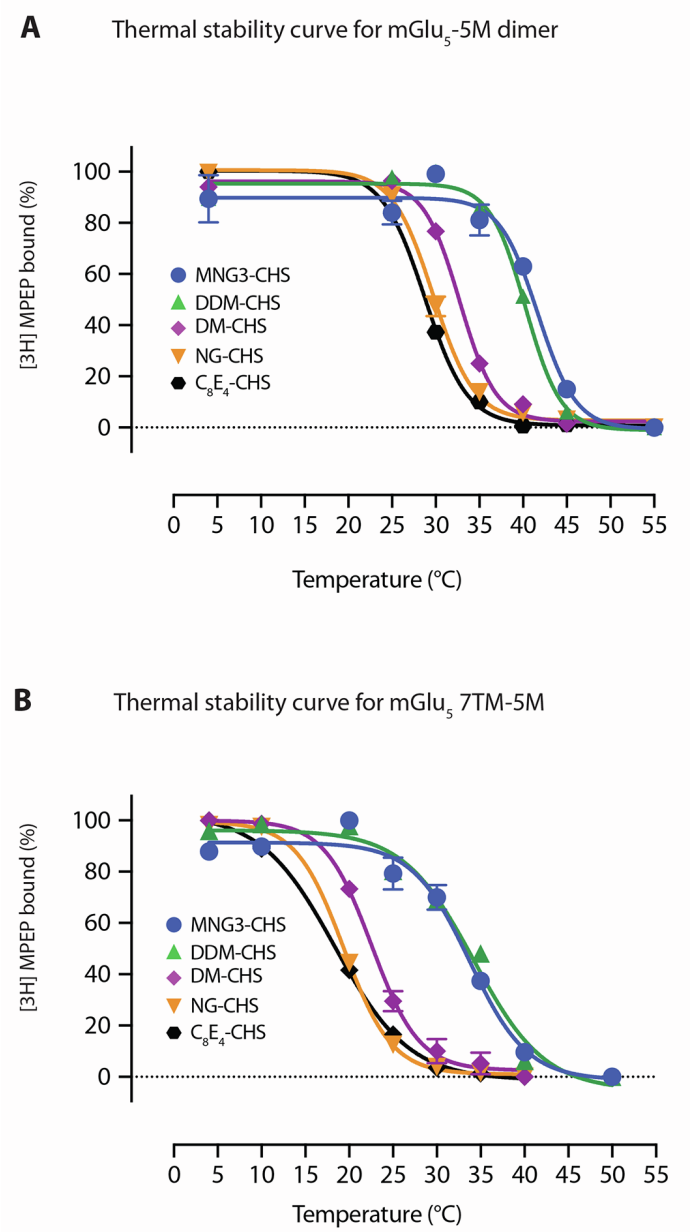

Figure S1. Thermal stability measurements of $mGlu_5$-5M receptor solubilised in detergents, Related to Figure 1 and Table S2. (A) Thermostability of the $mGlu_5$-5M dimer was measured using [^{3}H]-MPEP binding assay after extraction in different detergents including C_8E_4 (Black), NG (Orange), DM (Magenta), DDM (Green) and MNG3 (Blue), all supplemented with CHS. (B) Thermostability of the 7TM domain of $mGlu_5$-5M was measured for the same set of detergents. Experiments were performed in duplicates and each curve represents the average of three independent experiments with the exception of C_8E_4 for the $mGlu_5$-5M construct. T_m mean values are presented in Table S2.

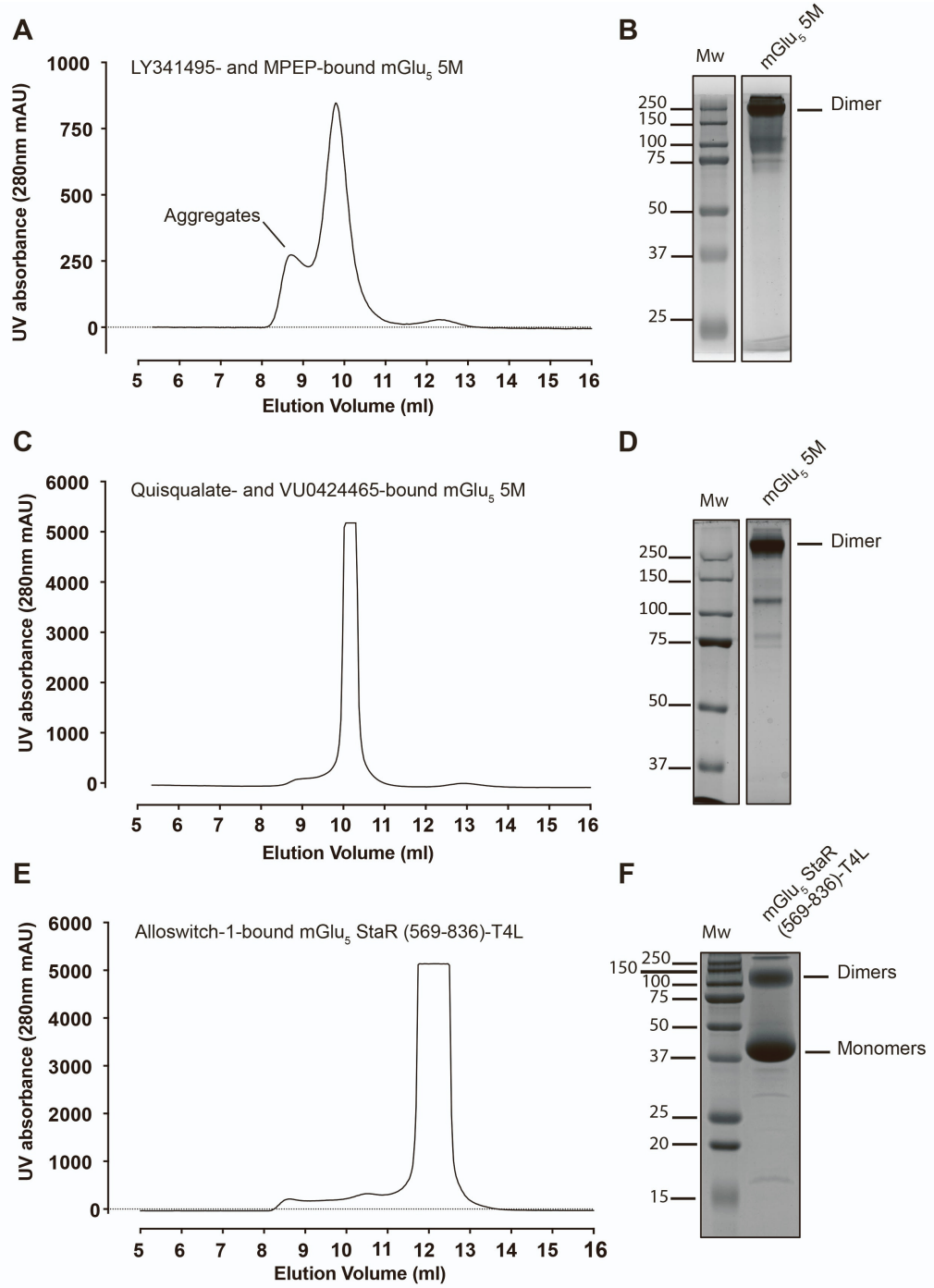

Figure S2. Size exclusion chromatography and SDS-gel of detergent-purified thermostabilised $mGlu_5$ receptor, Related to Figure 2 and Figure 4. Size exclusion chromatography was performed using 24 ml S200 column for thermostabilised $mGlu_5$-5M dimer bound to inhibitors (A), activators (C) and $mGlu_5$-StaR(569-836)-T4L bound to alloswitch-1 (E). 10% SDS-gel electrophoresis of purified thermostabilised $mGlu_5$-5M dimer bound to antagonist and NAM (B), agonist and PAM (D) and 15% SDS-gel electrophoresis of purified $mGlu_5$-StaR(569-836)-T4L bound to alloswitch-1 (F).

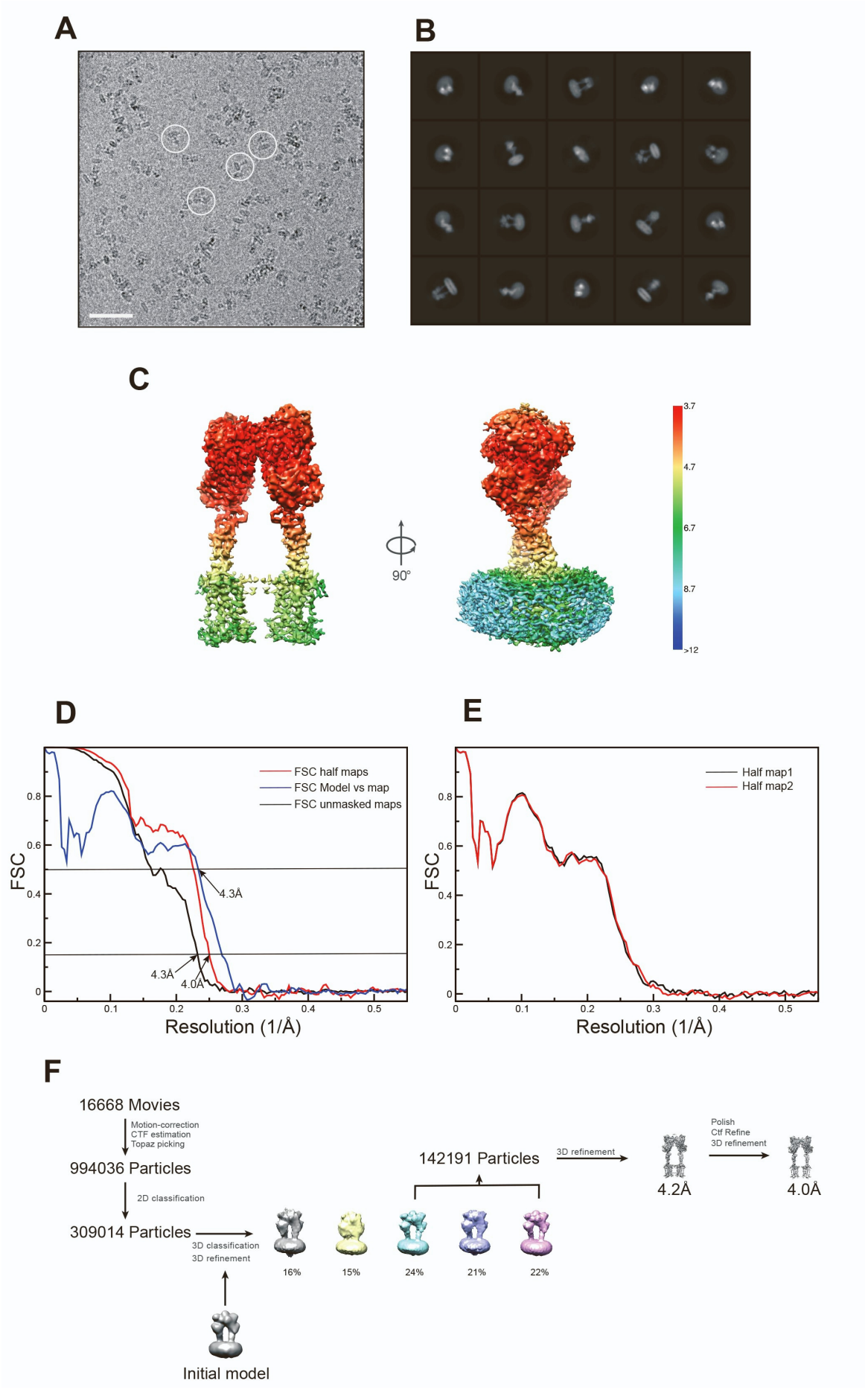
A
B
C
90°
3.7
4.7
6.7
8.7
>12
D
FSC half maps
FSC Model vs map
FSC unmasked maps
4.3Å
4.3Å
4.0Å
FSC
Resolution (1/Å)
E
Half map1
Half map2
FSC
Resolution (1/Å)
F
16668 Movies
Motion-correction
CTF estimation
Topaz picking
994036 Particles
2D classification
309014 Particles
3D classification
3D refinement
Initial model
16%
15%
24%
21%
22%
142191 Particles
3D refinement
4.2Å
Polish
Ctf Refine
3D refinement
4.0Å

56

Figure S3. CryoEM analysis of LY341495 and MPEP-bound $mGlu_5$ conformation, Related to Figure 2. (A) A representative micrograph of antagonist and NAM bound $mGlu_5$ in detergent micelles on ice. Scale bar is 500Å. (B) A selection of reference-free 2D class averages of $mGlu_5$ in antagonist bound conformation showing the distinct domains of the protein. The box size is 128 pixels and sampled at 3.56 Å. (C) Local resolution plot of antagonist $mGlu_5$ bound as determined with Relion 3.1. Two different views of the maps are shown at different thresholds. The molecule on the right has been rotated to show a different view of $mGlu_5$ and is at lower threshold. The lower threshold where the 7TM is covered by the detergent/lipid belt and the higher threshold showing the helices of the 7TM. Much of the VFT is between resolutions of 3.7 to 5 Å but the C-terminal part of CRD and the 7TM are of lower resolution. (D) The Fourier shell correlation (FSC) curves of two half-maps with mask (blue), unmasked maps (black) and the map and model (red) are shown. The estimated resolution by comparison of the two half-maps from refinement and postprocessing at FSC 0.143 is 4.0 Å and the one of map vs model at FSC 0.5 is 4.3 Å. The FSC curves were estimated for the full molecule. (E) To verify overfitting of the model refinement, one of the half-map used in refinement and the other half-map was used as test. (F) The CryoEM workflow showing the different steps used to obtain the final map.

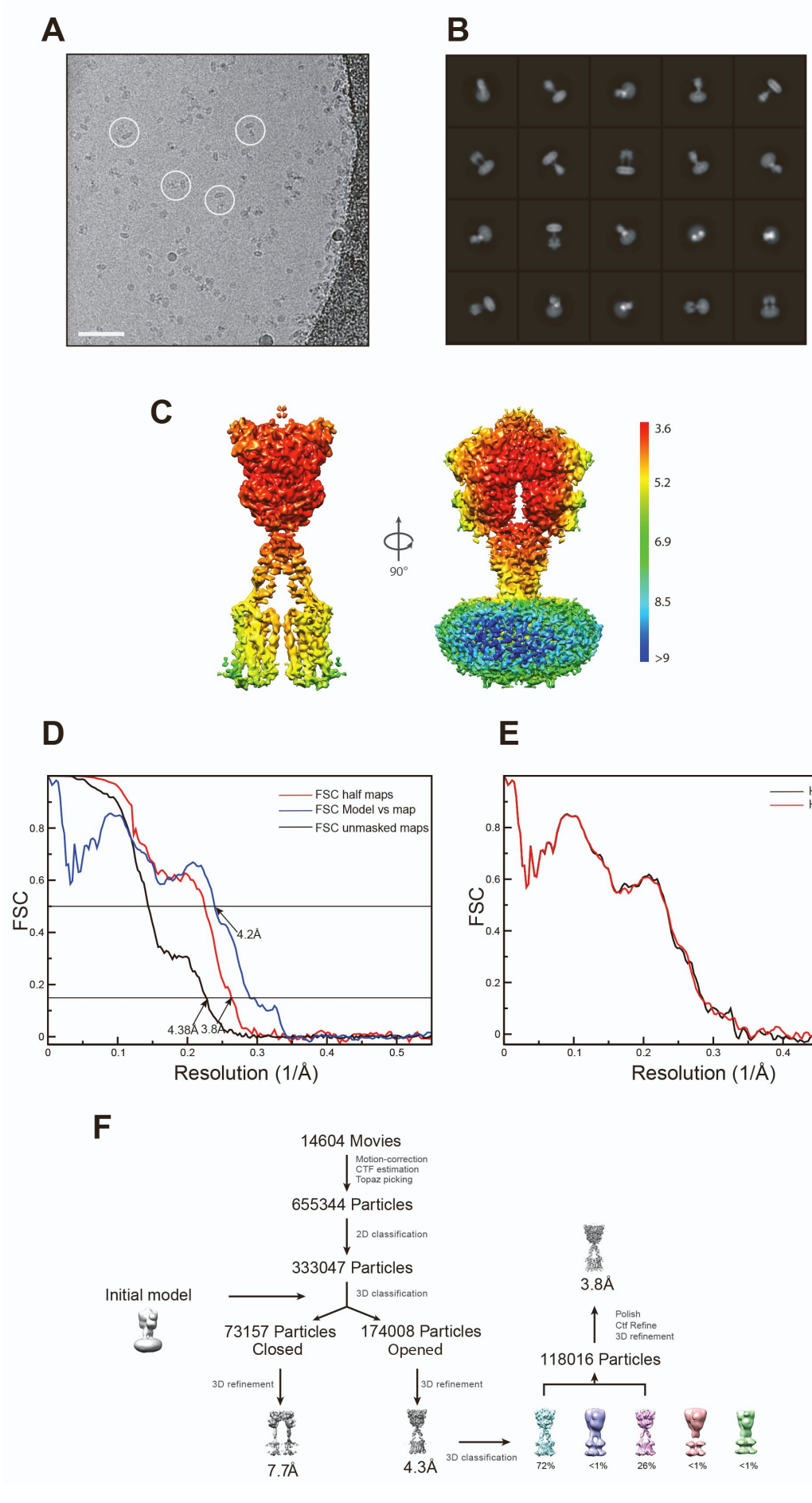
A
B
C
90°
3.6
5.2
6.9
8.5
>9
D
FSC half maps
FSC Model vs map
FSC unmasked maps
4.2Å
4.38Å 3.8Å
FSC
Resolution (1/Å)
E
Half map1
Half map2
FSC
Resolution (1/Å)
F
14604 Movies
Motion-correction
CTF estimation
Topaz picking
655344 Particles
2D classification
333047 Particles
Initial model
3D classification
73157 Particles
Closed
174008 Particles
Opened
3D refinement
3D refinement
7.7Å
4.3Å
3D classification
72%
<1%
26%
<1%
<1%
118016 Particles
Polish
Ctf Refine
3D refinement
3.8Å

76

Figure S4. Cryo EM analysis of quisqualate and VU0424465-bound $mGlu_5$ conformation, Related to Figure 2. (A) A representative micrograph of agonist and PAM bound $mGlu_5$ in detergent micelles on ice. Scale bar is 500 Å. (B) A selection of reference-free 2D class averages of $mGlu_5$ in closed conformation showing the distinct domains of the protein. The box size is 128 pixels and sampled at 3.56 Å. (C) Local resolution plot of $mGlu_5$ bound to quisqualate as estimated with Relion 3.1. Two different views of the maps are shown at different thresholds that hides detergent belt. The molecule on the right shows a rotated view of $mGlu_5$. Much of the VFTs are between resolutions of 3.6 to 5 Å but the C-terminal part of CRDs and the 7TMs are of lower resolution. (D) The Fourier shell correlation (FSC) curves of two half-maps with mask (blue), unmasked maps (black) and the map and model (red) are shown. The estimated resolution by comparison of the two half-maps from refinement and postprocessing at FSC 0.143 of half-maps is 3.8 Å and that of the map vs model at FSC 0.5 is 4.2 Å. The FSC curves were estimated for the full molecule. (E) Cross-validation of model refinement. To verify overfitting of the model refinement, one of the half-map used in refinement and the other half-map was used as test. (F) The CryoEM workflow showing the different steps used to obtain the final map.

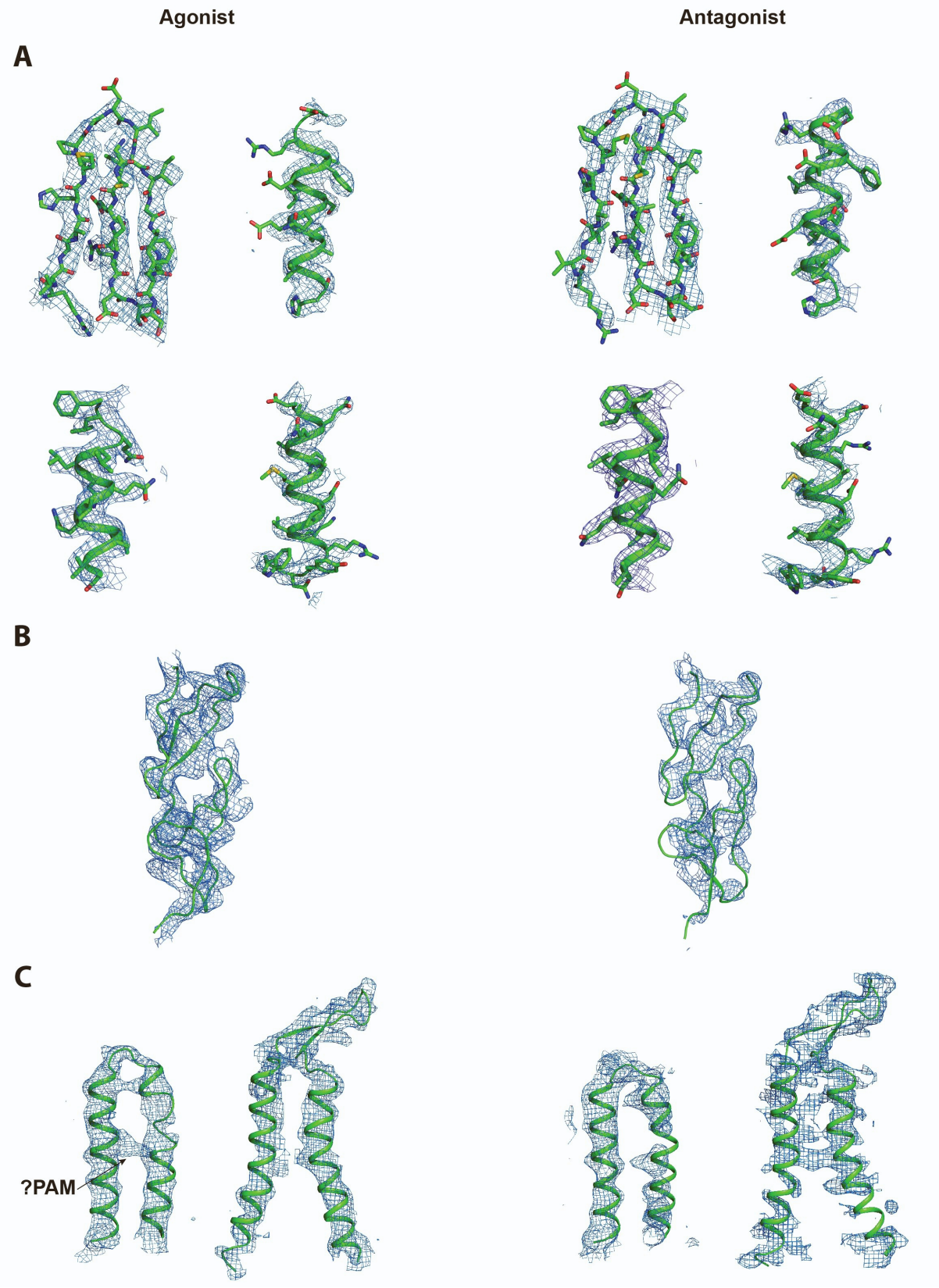

Figure S5. EM maps of select regions of full-length $mGlu_5$-5M bound to agonist (quisqualate) and antagonist (LY341495), Related to Figure 2. (A) α-helical and β-sheet regions from the VFT domain. The regions from each model include residues 26-42, 92-98 (β-sheet), 101-116,

153-165, 195-211 (α-helices). EM maps sharpened with B-factor of -122 Å^2 and -164 Å^2 for agonist and antagonist respectively were used to represent the density using Pymol. (B) The region comprising the CRD is shown. Only the backbone of the model is depicted due to lower resolution. EM maps sharpened with B-factor of -61 Å^2 and -82 Å^2 for agonist and antagonist respectively was used for depiction of maps using Pymol. (C) Two stretches of residues (690-760, 775-818) in the 7TM for agonist and antagonist are shown. In the agonist map, the extra density observed between the two helices, which is most likely the ligand PAM used in the preparation is marked with black arrow. The density for 7TMs of agonist is better than the antagonist and is clearly visualised in the maps. The docking of the TMD into the EM maps was aided by the X-ray structure of the 7TM. EM maps sharpened with B-factor of -61 Å^2 and -82 Å^2 for agonist and antagonist respectively was used for display of maps using Pymol.

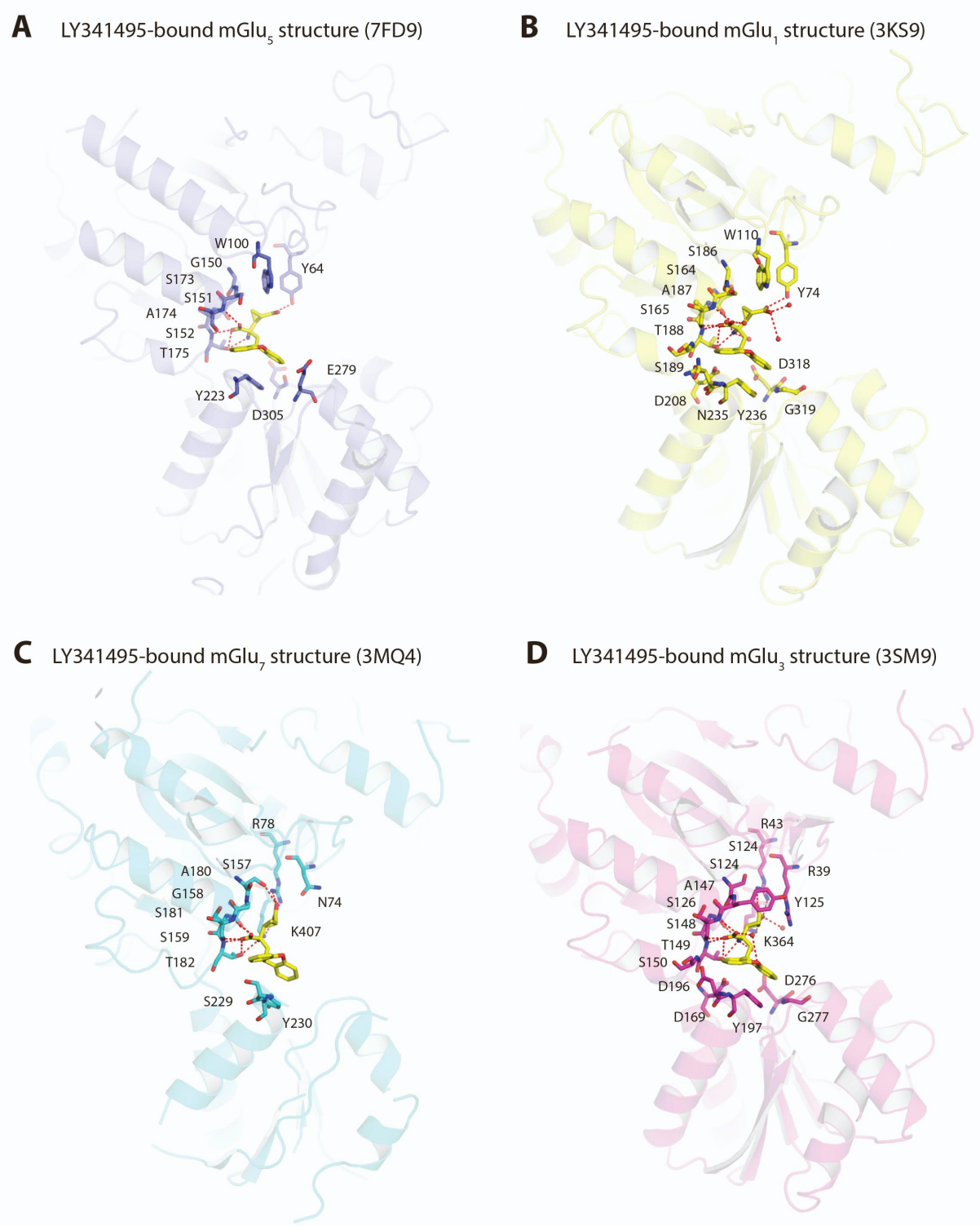

Figure S6. Comparison of the LY341495 binding site in the VFT of mGlu receptors that belongs to three different groups, Related to Figure 3. (A) The LY341495 binding to $mGlu_5$ pocket observed from this work and belongs to the group I, (B) from the $mGlu_1$ structure (PDB 3KS9) that belongs to the same group, (C) $mGlu_7$ structure (PDB 3MQ4) that belongs to group III and (D) $mGlu_3$ structure (PDB 3SM9) that belongs to group II.

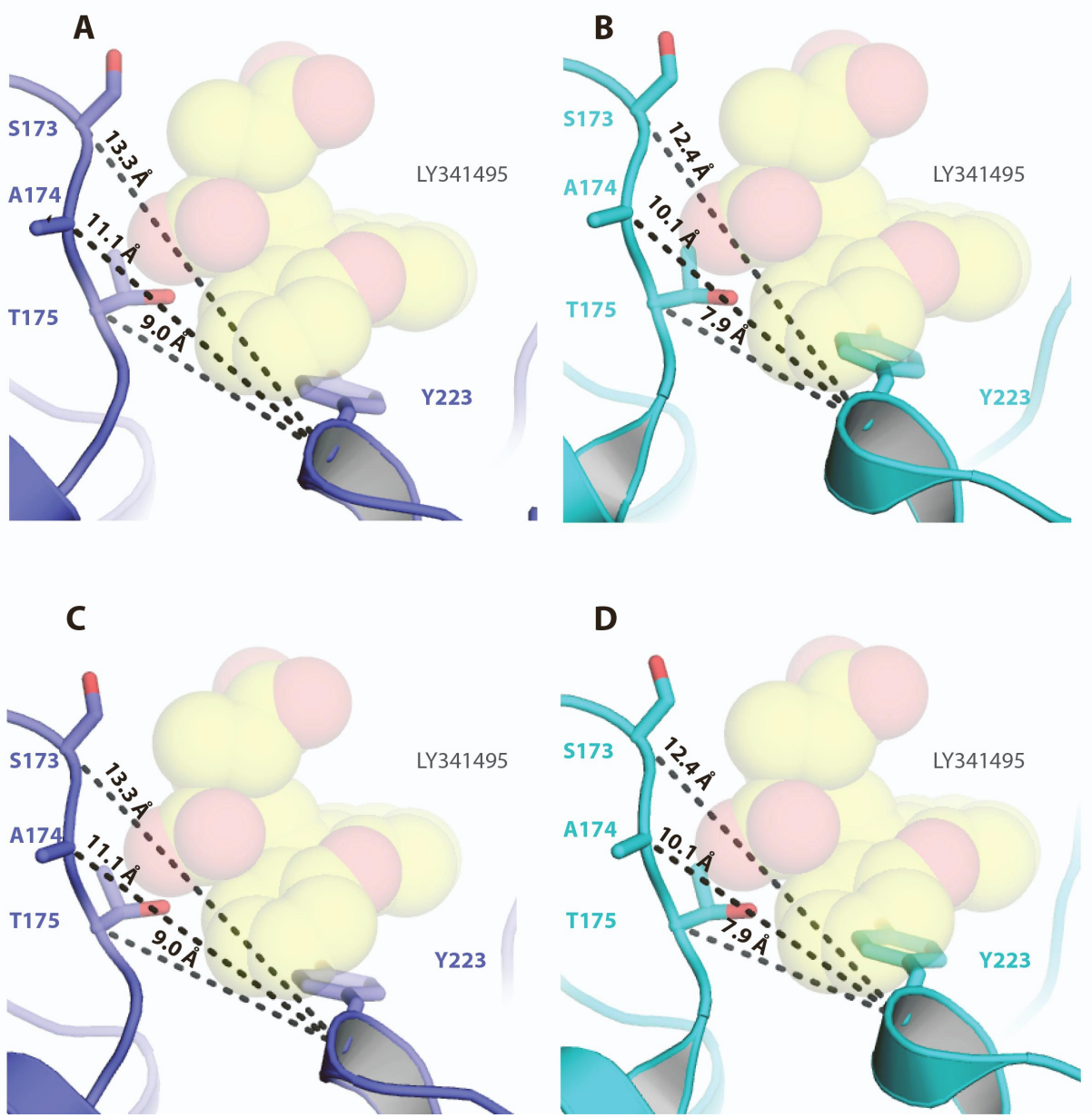

Figure S7. Binding of LY341495 is likely to require a larger opening of the VFT, Related to Figure 3. (A-D) Distances between Cα of the Y223 in lobe II and T173, A174 and S175 in lobe1 of protomer A (shown in panels A and B) and protomer B (shown in panels C and D). LY341494-bound $mGlu_5$ model is represented in blue (A and C) and apo inactive conformation (PDB 6N52) in cyan (B and D).

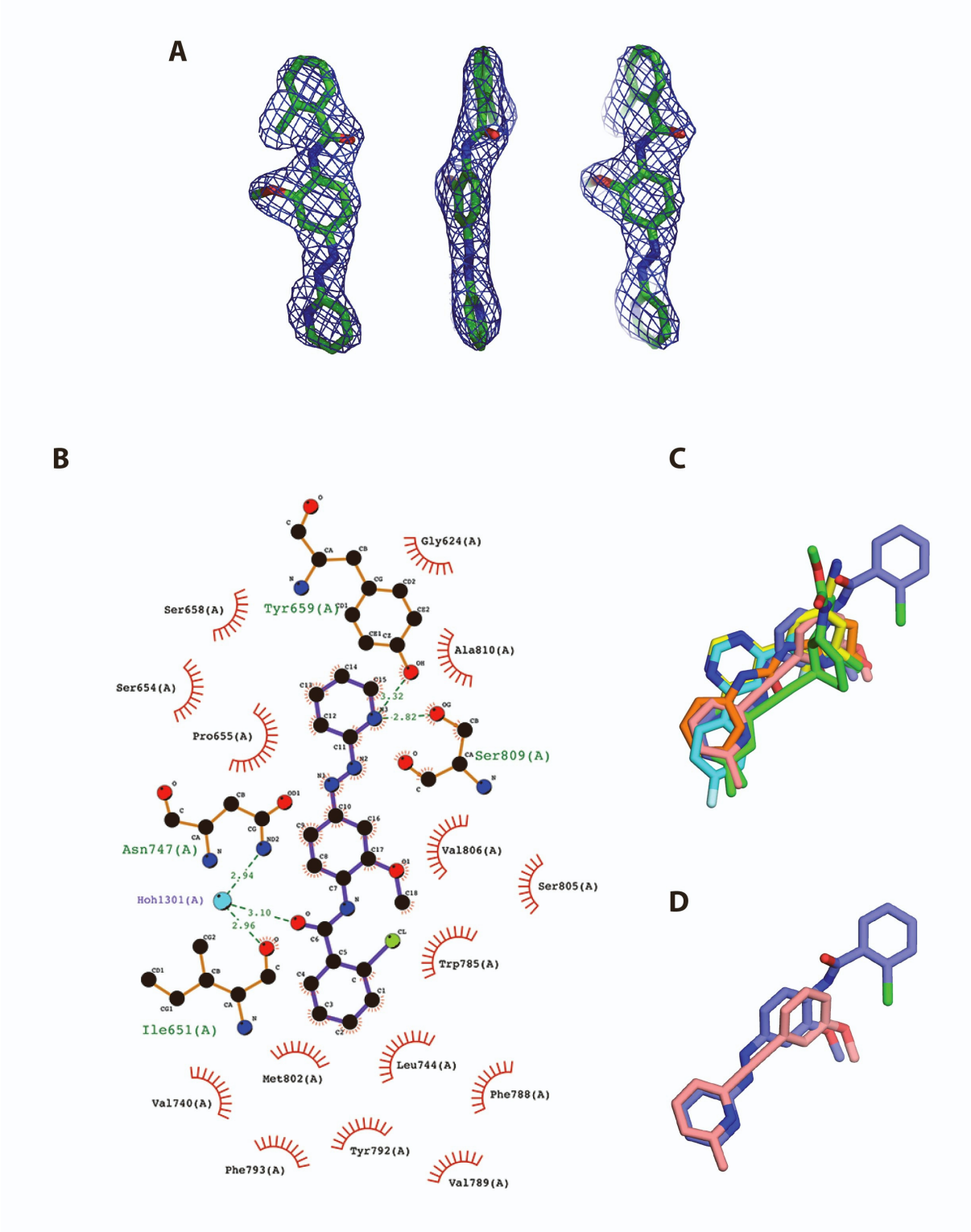

123

124 **Figure S8.** Alloswitch-1 binding mode in the 7TM domain of the $mGlu_5$ 7TM, Related to
125 Figure 4. (A) 2Fo-Fc map for alloswitch-1 bound to the thermostabilised 7TM domain of the
126 human $mGlu_5$ receptor. Map was calculated using Refmac and figure made with pymol at 1.5
127 σ. (B) 2D representation of Alloswitch-1 ligand binding site. 2D plot was generated using
128 LigPlot$^+$. (C) Alloswitch-1 superposition with the NAM co-crystallised with the $mGlu_5$ Star

7TM domain. Alloswitch-1 superposition with Mavoglurant (Green; 4OO9), M-MPEP (Light pink; 6FFI), Fenobam (Orange; 6FFH), HTL14242 (Cyan; 5CGD), HTL14242 derivative (yellow; 5CGC), Alloswitch-1 (Purpleblue; 7P2L). NAMs are coloured as indicated in brackets along with the PDB code. (D) Alloswitch-1 superposition with M-MPEP.

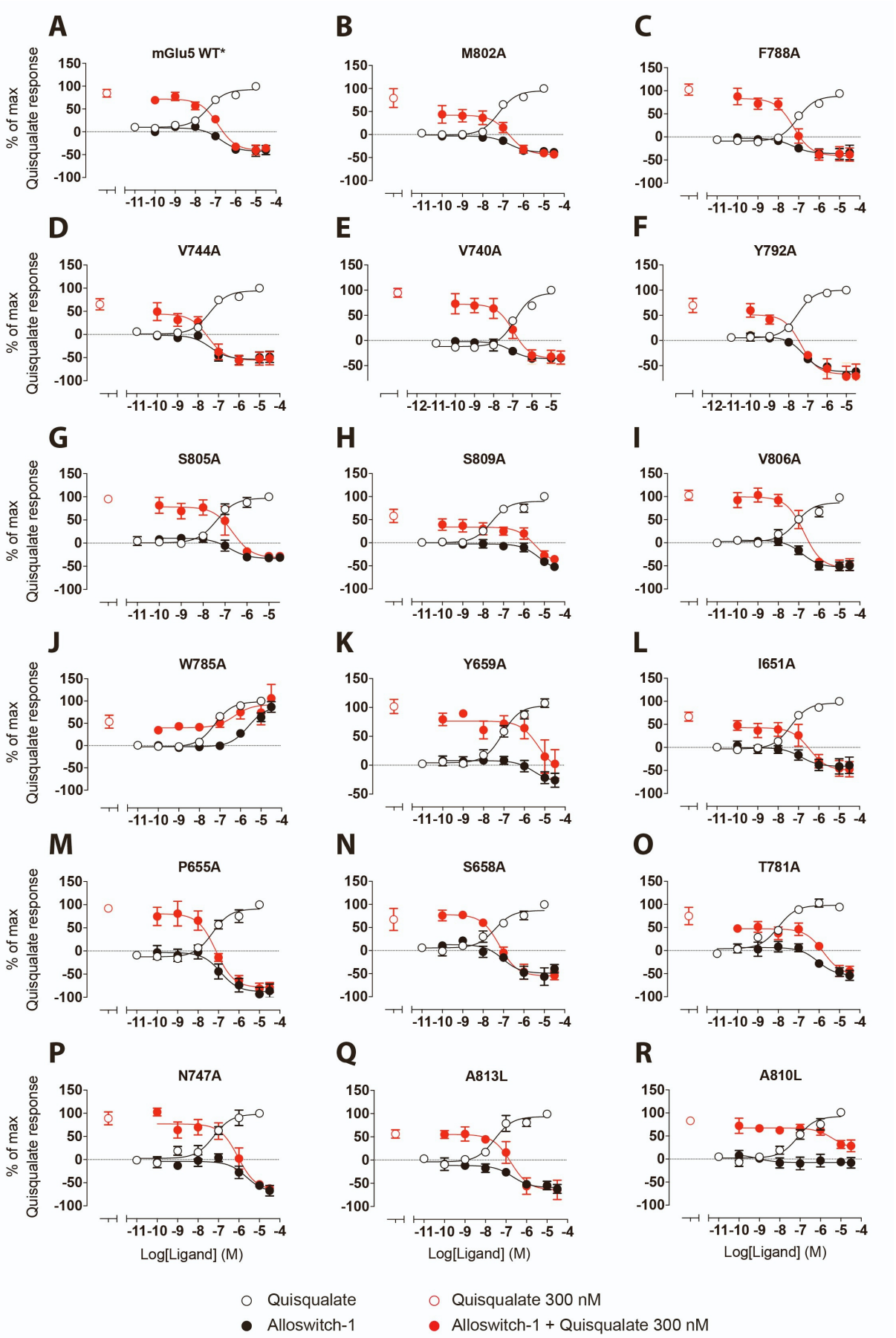
A
mGlu5 WT*
B
M802A
C
F788A
D
V744A
E
V740A
F
Y792A
G
S805A
H
S809A
I
V806A
J
W785A
K
Y659A
L
I651A
M
P655A
N
S658A
O
T781A
P
N747A
Q
A813L
R
A810L
% of max Quisqualate response
Log[Ligand] (M)
Quisqualate
Alloswitch-1
Quisqualate 300 nM
Alloswitch-1 + Quisqualate 300 nM

134

Figure S9. Probing the quisqualate and alloswitch-1 binding sites of $mGlu_5$ under dark conditions with IP_1 accumulation assay, Related to Figure 4. (A-R) Quisqualate-induced IP_1 accumulation (open circles) and alloswitch-1 inhibition of IP_1 accumulation in the presence (red circles) or absence (black circles) of a fixed concentration of quisqualate (300 nM; red circle) for $mGlu_5$ mutants, under dark conditions. Single point mutations were tested for their response to quisqualate and/or alloswitch-1 function of the $mGlu_5$. Data are expressed as a percentage of the maximal quisqualate response and represent the mean ± S.E.M. of at least three independent experiments performed in duplicate.

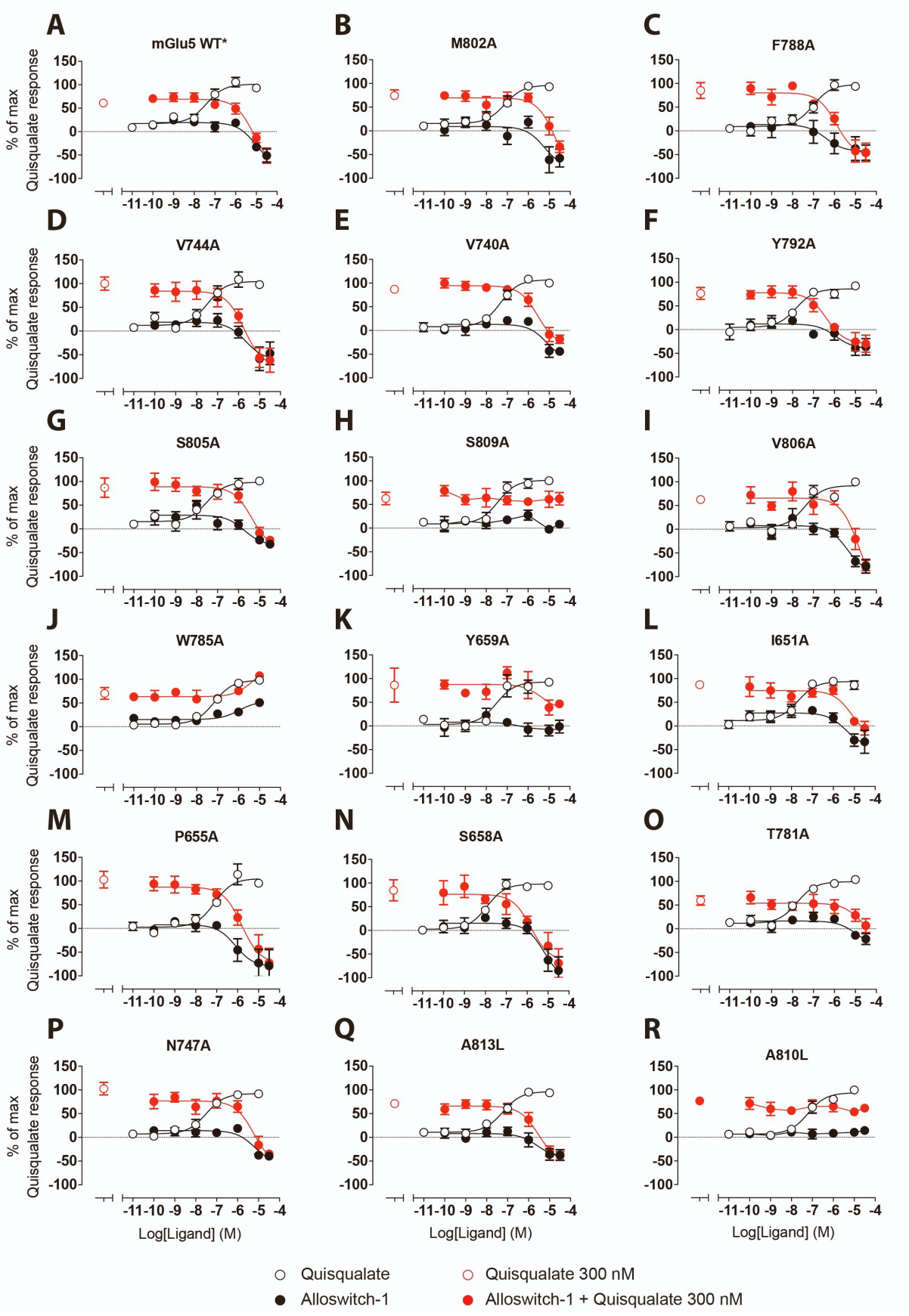

144

145 **Figure S10.** Probing the quisqualate and alloswitch-1 binding sites of $mGlu_5$ after illumination

146 with 380 nm light with IP_1 accumulation assay, Related to Figure 4. (A-R) Quisqualate-induced

147 IP_1 accumulation (open circles) and alloswitch-1 inhibition of IP_1 accumulation in the presence
148 (red circles) or absence (black circles) of a fixed concentration of quisqualate (300 nM; red
149 circles) for $mGlu_5$ mutants, under illuminated conditions. Single point mutations were tested
150 for their response to quisqualate and/or alloswitch-1 function at the $mGlu_5$ under 380 nm
151 conditions. Data are expressed as a percentage of the maximal quisqualate response and
152 represent the mean ± S.E.M. of at least three independent experiments performed in duplicate.
153

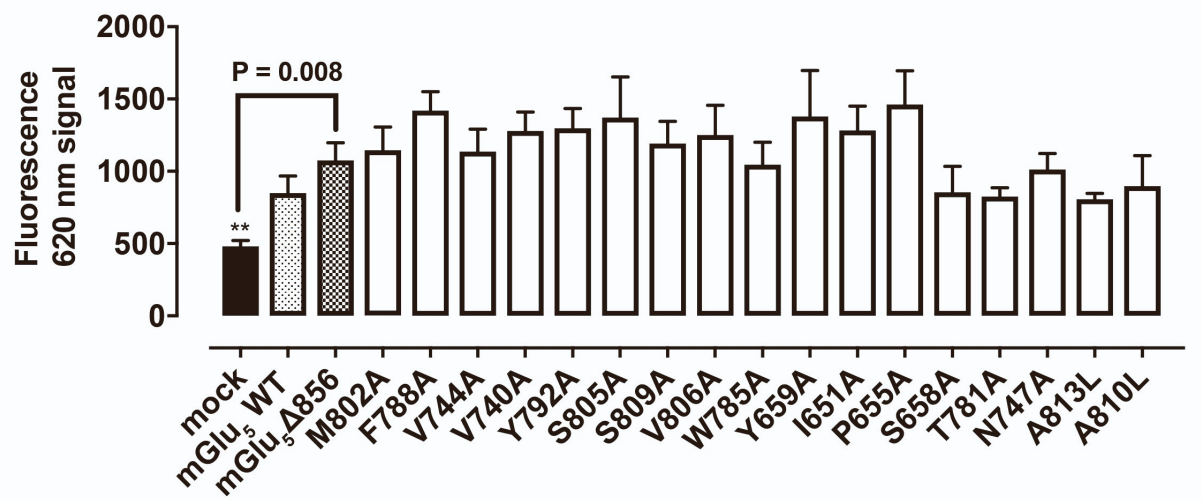

Figure S11. Quantification of cell surface expression of fluorescently labelled SNAP-tagged wildtype or mutant $mGlu_5$ receptors, Related to Figure 4. Data are expressed as the mean ± S.E.M. of at least three separate experiments performed in either duplicate or triplicate. Data were analysed with a one-way ANOVA with post-hoc Dunnett's multiple comparison's test. **P<0.01 denotes significant difference in cell surface expression from the mGlu5 WT receptor expressing cells.

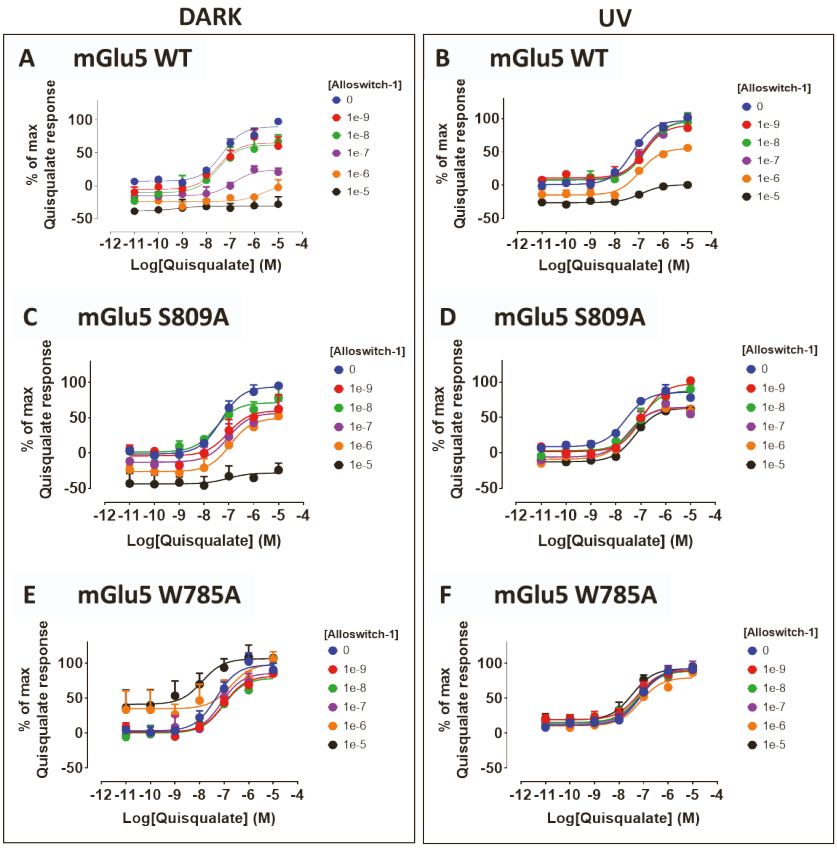

161

162 **Figure S12.** Interaction of the photoswitchable NAM, alloswitch-1, with the orthosteric
163 agonist, quisqualate, with $mGlu_5$ mutants in IP_1 accumulation assay, under dark or 380 nm
164 conditions, Related to Figure 4. (A, B) The response of WT $mGlu_5$ to alloswitch-1 in dark or
165 380 nm conditions are shown. The effect of the single point mutations $S809A^{7.39}$ (C, D) or
166 $W785A^{6.50}$ (E, F) on the ability of alloswitch-1 to inhibit quisqualate-induced IP_1 accumulation
167 in a concentration dependent manner was determined and compared to $mGlu_5$ WT, under dark
168 and 380 nm conditions. Data are expressed as a percentage of the maximal quisqualate response
169 and represent the mean ± S.E.M. of at least three independent experiments performed in
170 duplicate.

Table S1. Thermostability of human $mGlu_5$ mutants bound to the negative allosteric modulator MPEP, Related to Figure 1. The best single thermostable mutants A813L ($mGlu_5$-1M ; TM7) was first selected and used as a platform for combining additional thermostable mutants in the following sequence order, T742A (TM5), S753A (TM5), T777A (TM6), and I799A (TM7). For each receptor mutants, $mGlu_5$-1M, $mGlu_5$-2M, $mGlu_5$-3M, $mGlu_5$-4M and the final thermostable mutant, $mGlu_5$-5M, T_m are expressed as the mean value from at least 3 independent experiments (± SEM), or ± SD for the mean of 2 independent experiments.

Mutants name	$mGlu_5$ mutations	Apparent T_m in MNG3 (°C)
$mGlu_5$-Δ856	-	20.7 ± 0.5, (n=12)
	R668A	22.9 ± 0.3, (n=2)
	T742A	24.1 ± 1.3, (n=6)
	G748A	22.6 ± 0.4, (n=2)
	G794A	23.2 ± 0.1, (n=2)
	S753A	21.5 ± 0.2, (n=2)
	A787L	25.3 ± 0.2, (n=3)
	T777A	24.1 ± 1.0, (n=2)
	I799A	26.5 ± 0.9, (n=3)
$mGlu_5$ -1M	A813L	28.0 ± 1.2, (n=4)
	A855L	22.4 (n=1)
	A856L	23.4 ± 0.9, (n=2)
$mGlu_5$ -2M	A813L/T777A	32.5 ± 0.5, (n=4)
$mGlu_5$ -3M	A813L/T777A/S753A	34.5 ± 1.3, (n=3)
$mGlu_5$ -4M	A813L/T777A/S753A/I799A	37.0 ± 1.0, (n=2)
$mGlu_5$ -5M	A813L/T777A/S753A/I799A/T742A	39.5 ± 0.6, (n=5)

Table S2. Detergent-thermostability comparison between the human $mGlu_5$-5M dimer and 7TM-$mGlu_5$-5M, both bound to the negative allosteric modulator MPEP, Related to Figure 1. Apparent T_m values from each detergent are expressed as the mean ± SEM from at least three independent experiments performed in duplicates, with the exception of C_8E_4 for the $mGlu_5$-5M construct. All detergents are supplemented with CHS.

Solubilisation condition	$mGlu_5$ construct	Apparent T_m in detergents (^oC)
MNG3-CHS	$mGlu_5$-5M	41.42 ± 0.18, (n=3)
DDM-CHS	$mGlu_5$-5M	40.22 ± 0.24, (n=4)
DM-CHS	$mGlu_5$-5M	32.75 ± 0.33, (n=4)
NG-CHS	$mGlu_5$-5M	29.65 ± 0.32, (n=4)
C_8E_4-CHS	$mGlu_5$-5M	28.76 ± 0.23, (n=2)
MNG3-CHS	7TM-$mGlu_5$-5M	33.81 ± 0.36, (n=5)
DDM-CHS	7TM-$mGlu_5$-5M	34.26 ± 0.29, (n=4)
DM-CHS	7TM-$mGlu_5$-5M	22.70 ± 0.26, (n=4)
NG-CHS	7TM-$mGlu_5$-5M	19.42 ± 0.30, (n=5)
C_8E_4-CHS	7TM-$mGlu_5$-5M	18.16 ± 0.67, (n=4)

Table S3. Cryo-EM Statistics for map and model refinement, Related to Figure 2.

	PDB -7FD9, EMDB-31537 $mGlu_5$ + LY341495 +MPEP	PDB-7FD8, EMDB-31536 mGlu5 +quisqualate+VU0424465
Microscope	Titan Krios	Titan Krios
Operating voltage	300 kV	300 kV
Mode	EFTEM	EFTEM
Nominal magnification	130000x	130000x
Pixel size (Å)	0.89	0.89
Spot size	7	7
Beam size (µm)	0.9	1.05
C2 aperture (µm)	50	50
Objective aperture (µm)	100	100
Exposure time (sec)	5.2	9
Dose rate (e^-/p/s)	7.6	5.894
Fractions (# of frames)	32	48
Dose/frame (e^-/Å^2/s)	1.56	1.39
Total dose (e^-/Å^2)	49.9	67
No. of particles in final map	142191	118016
Resolution nominal (Å), FSC 0.143	4.0	3.8
Auto B-factor sharpening (Å^2)*	-164	-122
Refinement		
Starting models	7P2L**, 6n52,	7P2L**, 6n50, 6n51,
Model composition		
Number of chains	2	2
Protein (No. of atoms)	5698	6014
Ligands (NAG, CHS, Quisqualate, LY341495)	40	62
Model Refinement		
FSC @ 0.5 (Å)	4.3	4.2
Average B factor (Å^2)		
Overall	147.5	113.4
Protein	148.0	113.2
NAG	93.7	84.5
Quisqualate/LY341495	61.6	38.8
CHS	-	185.1
RMS deviations		
Bonds (Å)	0.006	0.006
Angles (°)	1.1	1.2
Validation		
Ramachandran Plot (favoured/outliers)	93.6/0	91.3/0.13
Clash score	9.1	5.1
Molprobity score	1.9	1.8

*** The auto B-factor sharpened map was used for model refinement. For map interpretation/model building, maps sharpened with multiple B-factors were used**

**** - The 7TM used as template is the alloswitch-1 model in this study**

Table S4. Residues in the VFT binding sites for LY341495 and quisqualate in the $mGlu_5$ structure compared with binding site residues in mGlu1, 3 and 7, Related to Figure 3. Residues shown are within 4.0 Å of the ligand.

$mGlu_1$ PDB(3KS9)	$mGlu_5$ LY341495 (7FD9)	$mGlu_3$ (PDB 3SM9)	$mGlu_7$ (PDB 3MQ4)	$mGlu_5$ Quisqualate (7FD8)
Y74	Y64	R64	N74	Y64-
		R68	R78	
W110	W100			W100
G163	G150	S149	S157	
S164	S151	Y150	G158	S151
S165	S152	S151	S159	S152
S186	S173	A172	A180	S173
A187	A174	S173	S181	A174
T188	T175	T174	T182	T175
S189		S175		
D208		D194		
N235	N222	221	S229	
Y236	Y223	222	Y230	Y223
	E279			E279
				G280
D318	D305	D301		D305
G319		G302		G306
		K389	K407	K396

Table S5. Potency estimates for quisqualate-stimulated IP_1 accumulation or alloswitch-1 inhibition of IP_1 accumulation in the presence or absence of a fixed concentration of quisqualate (300 nM), under dark conditions at $mGlu_5$ mutations, Related to Figure 4. Estimated potency values represent the mean ± S.E.M. of at least three independent experiments performed in duplicate. Data were fitted to a standard logistic function and analysed by one-way ANOVA, with Dunnett's post-test. **P*<0.05, ***P*<0.01, ****P*<0.001, *****P*<0.0001 denotes significant difference of ligand potency at an $mGlu_5$-Δ856 as compared to the $mGlu_5$ WT receptor.

	Quisqualate pEC_{50} values (n)	Alloswitch-1 pIC_{50} values (n)	Alloswitch-1 pIC_{50} values, when interacted with 300 nM quisqualate (n)
mGlu5	7.52±0.18(4)	6.79±0.09(4)	6.66± 0.03(4)
$mGlu_5$-Δ856	7.30±0.10(9)	6.94±0.13(9)	7.07±0.17(9)
$I651A^{3.36}$	7.38±0.07(4)	6.90±0.13(4)	6.40±0.27(4)
$P655A^{3.40}$	7.39±0.11(3)	7.24±0.11(4)	6.97±0.27(4)
$S658A^{3.43}$	7.56±0.32(4)	7.27±0.26(4)	7.19±0.13(4)
$Y659A^{3.44}$	7.13±0.28(4)	5.73±0.54(4)**	5.28±0.36(3)****
$V740A^{5.40}$	6.90±0.09(4)	7.14±0.02(4)	7.08±0.16(4)
$L744A^{5.44}$	7.41±0.06(4)	7.30±0.06(4)	7.47±0.12(4)
$N747A^{5.47}$	7.31±0.16(4)	5.93±0.46(4)*	6.20±0.41(4)
$T781A^{6.46}$	8.13±0.24(4)**	6.06±0.15(4)	5.84±0.19(4)**
$W785A^{6.50}$	7.24±0.12(4)	5.50±0.09(4)***	5.72±0.43(3)**
$F788A^{6.53}$	7.03±0.06(4)	7.62±0.12(4)	7.48±0.23(4)
$Y792A^{6.57}$	7.55±0.06(4)	7.56±0.23(4)	7.60 ±0.22(4)
$M802A^{7.32}$	7.28±0.05(4)	6.80±0.19(4)	6.74±0.12(4)
$S805A^{7.35}$	7.39±0.08(4)	6.99±0.24(4)	6.75±0.23(3)
$V806A^{7.36}$	7.10±0.15(4)	7.19±0.37(4)	6.94±0.42(4)
$S809A^{7.39}$	7.39±0.23(4)	5.46±0.26(4)***	5.53±0.23(3)***
$A810L^{7.40}$	7.39±0.20(3)	n.d.	5.50±0.02(3)***
$A813L^{7.43}$	7.40±0.21(4)	6.93±0.42(4)	6.90±0.20

Table S6. Potency estimates for quisqualate-stimulated IP_1 accumulation or alloswitch-1 inhibition of IP_1 accumulation in the presence or absence of a fixed concentration of quisqualate (300 nM), under 380 nm conditions at $mGlu_5$ mutations, Related to Figure 4. Estimated potency values represent the mean ± S.E.M. of at least three independent experiments performed in duplicate. Data were fitted to a standard logistic function and analysed by one-way ANOVA, potency values were compared to the $mGlu_5$-Δ856 truncated in the C-terminus after Alanine 856.

	Quisqualate pEC_{50} values (n)	Alloswitch-1 pIC_{50} values (n)	Alloswitch-1 pIC_{50} values, when interacted with 300 nM quisqualate (n)
mGlu5	7.68±0.15(3)	4.48±0.12(3)	5.31±0.29(4)
$mGlu_5$-Δ856	7.56±0.12(8)	5.44±0.23(8)	5.58±0.24(8)
$I651A^{3.36}$	7.67±0.25(4)	5.39±0.20(4)	5.16±0.13(4)
$P655A^{3.40}$	7.17±0.10(4)	n.d.	n.d.
$S658A^{3.43}$	7.91±0.14(4)	5.51±0.35(4)	6.20±0.29(4)
$Y659A^{3.44}$	7.37±0.13(4)	6.21±0.32(4)	5.61±0.31(3)
$V740A^{5.40}$	7.32±0.17(4)	5.54±0.22(3)	6.07±0.75(3)
$L744A^{5.44}$	7.54±0.20(4)	5.68±0.15(4)	5.70±0.09(4)
$N747A^{5.47}$	7.73±0.24(4)	5.63±0.44(3)	5.70±0.31(4)
$T781A^{6.46}$	7.81±0.09(4)	n.d.	n.d.
$W785A^{6.50}$	7.30±0.17(4)	n.d.	n.d.
$F788A^{6.53}$	7.12±0.22(4)	5.93±0.20(4)	5.89±0.15(4)
$Y792A^{6.57}$	7.85±0.15(4)	6.16±0.59(4)	6.44±0.48(4)
$M802A^{7.32}$	7.42±0.10(4)	5.58±0.32(4)	4.92±0.43(4)
$S805A^{7.35}$	7.69±0.40(4)	5.84±0.17(4)	5.27±0.24(4)
$V806A^{7.36}$	7.25±0.22(4)	5.43±0.22(4)	4.92±0.19(2)
$S809A^{7.39}$	7.53±0.15(4)	n.d.	n.d.
$A810L^{7.40}$	7.22±0.20(4)	n.d.	n.d.
$A813L^{7.43}$	7.26±0.17(3)	5.76±0.38(3)	5.60±0.20(4)

Table S7. X-Ray Data collection and refinement statistics, Related to Figure 4.

PDB ID	**7P2L***
Space group	C2
a, b, c (Å)	141.69, 43.40, 82.12, 90, 99.384, 90
α, β. γ (°)	90, 90, 90
Beamline	SLS-X06SA
Wavelength (Å)	1.0
Resolution (Å)	41.45-2.54 (2.61–2.54)**
R*meas*	0.25 (2.68)
I /σ (I)	6.35 (1.05)
Completeness (%)	99.9 (100)
Multiplicity	10.66 (9.30)
CC1/2 (%)	0.99 (0.51)
Refinement	
Resolution (Å)	49.11-2.54
No. of unique reflections	16594
R_{work}/R_{free}***	0.23/0.28
R.m.s. deviations	
Bond lengths (Å)	0.01
Bond angles (°)	1.73
B-factor	
Total	75.0
Protein	75.2
Ligand	57.2
Water	60.1
Ramachandran Plot	
Favored (%)	95.5
Outliter (%)	0.25
Clash score	2.6
MolProbity score	1.4

* Data processing and refinement statistics are reported with Friedel pairs merged.
** Values in parentheses are for the highest resolution shell.
***R_{free} was calculated using 5% of randomly selected subset of reflections and the remaining 95% of reflections was used for calculation of R_{work}.

Table S8. Potency measurement for agonist quisqualate-stimulated and ago-PAM VU0424465 in IP_1 accumulation in the presence or absence of a fixed concentration of LY341495 (100 μM), Related to Figure 5. Values are the average +/- S.E.M from at least 3 different experiments.

	$mGlu_5$-Δ856 pEC_{50}
LY341495	5.51 ± 0.63 (n=3)
Quisqualate	6.83 ±0.16 (n=6)
Quisqualate + LY341495 (10^{-4}M)	5.27 ±0.05 (n=3)
VU0424465	7.47 ±0.08 (n=6)
VU0424465+ LY341495 (10^{-4}M)	6.82 ±0.05 (n=6)